

Incoherent neutron scattering and the dynamics of thin film photoresist polymers

Christopher L. Soles,^{a)} Jack F. Douglas, Eric K. Lin, Joseph L. Lenhart, Ronald L. Jones, and Wen-Li Wu

Polymers Division, National Institute of Standards and Technology, Gaithersburg, Maryland 20899-8541

Dario L. Goldfarb and Marie Angelopoulos

IBM T. J. Watson Research Center, Yorktown Heights, New York 10598

(Received 8 October 2002; accepted 25 November 2002)

Elastic incoherent neutron scattering is employed to parameterize changes in the atomic/molecular mobility in lithographic polymers as a function of film thickness. Changes in the 200 MHz and faster dynamics are estimated in terms of a harmonic oscillator model and the corresponding Debye–Waller factor mean-square atomic displacement $\langle u^2 \rangle$. We generally observe that relatively large $\langle u^2 \rangle$ values in the glassy state lead to a strong suppression of $\langle u^2 \rangle$ when the polymer is confined to exceedingly thin films. In contrast, this thin film suppression is diminished or even absent if $\langle u^2 \rangle$ in the glass is relatively small. We further demonstrate that highly localized side group or segmental dynamics of hydrogen-rich moieties, such as methyl groups, dominate $\langle u^2 \rangle$ and that thin film confinement apparently retards these motions. With respect to photolithography, we demonstrate that a reduced $\langle u^2 \rangle$ in exceedingly thin model resist films corresponds to a decrease in the reaction front propagation kinetics. © 2003 American Institute of Physics.

[DOI: 10.1063/1.1539538]

I. INTRODUCTION

It is well understood that segmental molecular motions, either along the backbone or localized to side groups, dramatically affect the kinetics of small molecule transport through polymeric materials.^{1,2} Specifically, several authors argue that these motions produce a gating effect that regulates gas, absorbate, or small molecule transport through the interchain regions of amorphous polymers.^{3–6} This effect should be of consequence in deep UV lithography where a photochemically generated acidic proton (H^+) diffuses through a photoresist film, inducing numerous chemical reactions. With an approximate diameter of 1 Å, H^+ should readily diffuse through typical amorphous polymers, in which the interchain distances (between atom centers) are on the order of 5 Å. However, it remains to be determined how the high frequency local chain motions, such as segmental vibrations, librations, rotations, etc., affect H^+ mobility in these interchain regions.

An understanding of how the dynamics in a polymer matrix couple to H^+ transport kinetics is crucial for sub-100 nm lithography. As device features continue to shrink in the microelectronics industry, there is a push to utilize exceedingly thin lithographic films. This is partially because printing small features into a thick film leads to high aspect ratios and problems of buckling or pattern collapse. Equally as important is the fact that printing sub-100 nm features necessitates a shift to shorter wavelength UV sources. State-of-the-art deep UV lithography tools utilize either 248 or 193 nm radiation, but in the near future, 157 nm radiation will be required to keep pace with the trend of shrinking device fea-

tures. However, there are considerable roadblocks to realizing 157 nm lithography. To properly produce a high resolution lithographic image the resist must be optically transparent to ensure uniform illumination throughout the entire thickness of the photoresist film. At 157 nm, most polymers strongly absorb. In addition chemical modification to enhance transparency (i.e., no aromatic groups, high fluorine content, etc.), it is possible to reduce absorption by minimizing the film thickness. So it should be apparent that as feature sizes continue to shrink, it will not be long before the thickness of the resist film is on the order of 100 nm or less. These length scales approach the unperturbed dimensions of the polymers in the resist, meaning that confinement issues must be considered. It is well known that thin film confinement can affect the basic thermophysical properties of polymeric materials, as summarized in several reviews and books.^{7–9}

We have recently shown it is possible to characterize thin film confinement-induced changes of the high frequency atomic motions with incoherent neutron scattering.^{10–12} The collection of atomic and molecular motions faster than 200 MHz can be parameterized in terms of the hydrogen-weighted, averaged mean-square atomic displacement $\langle u^2 \rangle$. Specifically, we showed that thin film confinement leads to a suppression $\langle u^2 \rangle$, or reduced local mobility on the nanosecond time scale. Since $\langle u^2 \rangle$ is less than few Å² in most solid polymers, it appears that the time and length scales are appropriate to capture the dynamics germane to H^+ mobility and the photolithography process. Specifically, in this article we will demonstrate that the confinement-induced $\langle u^2 \rangle$ changes in a series of lithographic thin films correlate with a

^{a)}Electronic mail: csoles@nist.gov

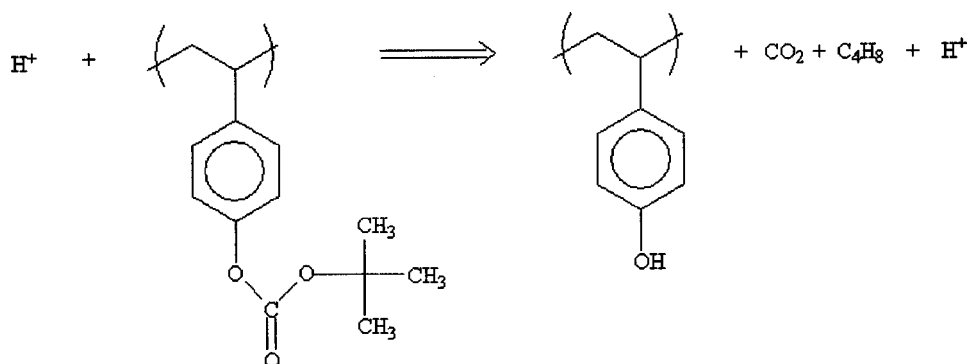


FIG. 1. Chemical structures and simplified reaction scheme indicating that PBOCSt reacts with the photoacid (H^+) to form PHOSt, carbon dioxide, isobutylene, and a regenerated acid.

documented reduction of the photoacid mobility in exceedingly thin photoresist films.

II. EXPERIMENT

A. Samples

Incoherent neutron scattering experiments were performed on the model 248 nm resist formulation: poly(*tert*-butoxycarboxystyrene) (PBOCSt) and poly(4-hydroxystyrene) (PHOSt). While this resist will not be utilized for sub-100 nm lithography because of transparency limitations, it is a widely studied system and therefore suitable for demonstrating our technique. PHOSt ($M_{n,r} = 8000$ g/mol) was purchased from Triquest.¹³ The protected analog was created by attaching *t*-butylene 4-vinylphenyl carbonate (Aldrich) onto the 4 position of the phenol ring via free radical polymerization.¹⁴ The chemical structures are identified in Fig. 1, along with the reaction whereby the base-insoluble PBOCSt is converted into the base-soluble PHOSt through the action of the H^+ photoacid. Deprotection consumes the *tert*-butylcarboxy group, volatilizing it into CO_2 and isobutylene (which leave the sample).

To isolate the dynamical contributions of the bulky protecting group, a deuterium substituted *tert*-butylcarboxy group was utilized. The incoherent neutron scattering signal is dominated by the hydrogenous moieties in most polymers. Hydrogen has an incoherent neutron scattering cross section nearly 40 times larger than that of deuterium (as well as of most other elements commonly found in hydrocarbon polymers). Deuterium labeling effectively masks the dynamics of the *tert*-butylcarboxy group, separating the $\langle u^2 \rangle$ contributions from the polymer backbone and the protecting side group. The procedure for synthesizing the deuterium-labeled dPBOCSt is described elsewhere.¹⁵

The PBOCSt and PHOSt were dissolved in propylene glycol methyl ether acetate at various mass loadings. All solutions were filtered through a 0.45 μm Teflon filter and spun cast at 2000 rpm onto thin $\langle 100 \rangle$ Si wafers with 75 mm diameters. Prior to spin casting, any organic contaminants were cleaned off the wafers using an O_2 plasma. The native silicon dioxide surface was etched away with HF acid, and then regrown as a uniform (5–10) \AA thick oxide layer through a 5 min exposure in an UV ozone chamber. This creates a visibly hydrophilic surface. After spin casting, excess solvent was removed through a 12 h postapply bake at 120 $^\circ C$ under vacuum of 0.1 Pa or better. We have confirmed

that these conditions are not sufficient to induce significant thermal deprotection. Prior to the neutron scattering measurements, the sample thickness was determined by x-ray reflectivity. For the experiments described here, the film thickness varied from 1340 to 83 \AA , with the bulk measurement performed on the solvent free, precipitated polymer powders.

B. Methods

The incoherent neutron scattering measurements were performed on the high flux backscattering spectrometer (HFBS) on the NG2 beamline at the National Institute of Standards and Technology (NIST) Center for Neutron Research.¹⁶ These types of thin film scattering experiments, described elsewhere in detail,^{10,12} utilize the fixed window mode (stationary Doppler drive) of the spectrometer to record the incoherent elastic scattering intensities I_{elastic} as a function of Q , where $Q = 4\pi \sin(\theta)/\lambda$, θ is the scattering angle, and λ the neutron wavelength. The Q dependence of the elastic scattering is analyzed within the framework of the Debye–Waller harmonic approximation. In this model,

$$I_{\text{elastic}}(Q) \propto e^{(-1/3)Q^2 \langle u^2 \rangle}, \quad (1)$$

with $\langle u^2 \rangle$ denoting the hydrogen-weighted mean-square atomic displacement. Within this approximation $\langle u^2 \rangle$ is defined by the linear slope of $\ln[I_{\text{elastic}}(Q)]$ vs Q^2 . As the thermal motions become excited, there is a decrease in the intensity of the elastically scattered neutrons and correspondingly an increase in $\langle u^2 \rangle$. The analysis is analogous the broadening of x-ray diffraction peaks that occurs with temperature in a crystalline material. Because these are not truly inelastic neutron scattering measurements, we are not able to directly quantify the time scale of the dynamics. However, given the 0.85 μeV energy resolution of the spectrometer, we know that only motions faster than 200 MHz lead to an increase of $\langle u^2 \rangle$; slower motions are seen as elastic scattering.

To maximize the scattering signal, 13–15 identical wafers were broken into approximately (20 \times 50) mm² strips and contained in the thin walled aluminum sample cells for the HFBS spectrometer. Depending on the film thickness, this corresponded to (0.5–10.0) mg of polymer in the cell in contrast to approximately 50 g of Si. Despite the limited mass, it is important to realize that the polymer still dominates the scattering. First the Si wafers and Al sample cell are both virtually transparent to the neutrons in terms of their absorption cross sections. Furthermore, Si and Al are crys-

talline and elastic scattering can only occur at certain reflections. The fact that the Q range of the HFBS spectrometer, $0.25 \text{ \AA}^{-1} < Q < 1.75 \text{ \AA}^{-1}$, is below the Bragg diffraction peaks of the Si and Al absolutely ensures that $\langle u^2 \rangle$ reflects the dynamics of the polymer. Finally, it is also important to realize that the scattering cross section of H is approximately 40 times greater than those of typical C or O found in most polymers. This implies that $\langle u^2 \rangle$ will be heavily weighted towards the motions of the hydrogenous moieties in the polymer.

The HFBS cell containing the films was mounted on the spectrometer, evacuated, and cooled to 40–50 K. After equilibration, the temperature was ramped linearly to 500 K at rates ranging from 1.0 (for the bulk samples) to 0.1 K/min (for the thinnest films), with the elastic intensities binned (summed) into intervals of 1–3 K. At each temperature interval, $\langle u^2 \rangle$ was calculated using Eq. (1) and the Q dependence of the elastic scattering.

III. RESULTS

Figure 2 demonstrates the thermal evolution of the elastic scattering for both the PHOSt and PBOCSt samples. As thermal motions are introduced into the sample there is a gradual reduction in the scattering intensity. The total elastic intensities, summed over the entire Q range of the spectrometer, in Fig. 2(a) are normalized by their values at 50 K so that films of different thickness can be directly compared. In this representation the reduction of I_{elastic} as the film thickness decreases indicates a loss of mobility, an effect that is more pronounced in the PBOCSt films compared into PHOSt ones.

PBOCSt also shows a precipitous decrease in I_{elastic} near 410 K, which corresponds to a thermal induction (without photoacid) of the deprotection reaction in Fig. 1. There are two possible reasons for the sudden reduction of I_{elastic} . First, the sample loses mass (as CO_2 and isobutylene) during the reaction, which should lead to sudden decrease in the scattering intensity. However, the discontinuous decrease upon deprotection is limited to the low Q detectors, as seen in Fig. 2(b) (PBOCSt) [and not observed in PHOSt, Fig. 2(c)]. If mass loss alone were the cause of the sudden drop of intensity, it should be observed in both the low and high Q detectors. The fact that there are no discontinuities in the high Q detectors in Fig. 2(b) is because the sample cell is sealed and the gaseous by-products are not able to readily escape into the vacuum. With regard to the energy resolution of the spectrometer, the methyl groups are already dynamic (not contributing to the elastic scattering) at 400 K so it is somewhat immaterial from the perspective of the spectrometer if they are in gaseous or solid form. Rather, the conversion of PBOCSt to PHOSt is accompanied by a pronounced change in the static structure factor (scattering) below $Q = 0.5 \text{ \AA}^{-1}$. This is reasonable since amorphous polymers with large side groups (like PBOCSt) can have low Q correlation peaks in this region, while those without (like PHOSt) do not.¹⁷ Preliminary neutron diffraction measurements indicate that this is an appropriate explanation. The large reduction in intensity at low Q primarily reflects structural changes

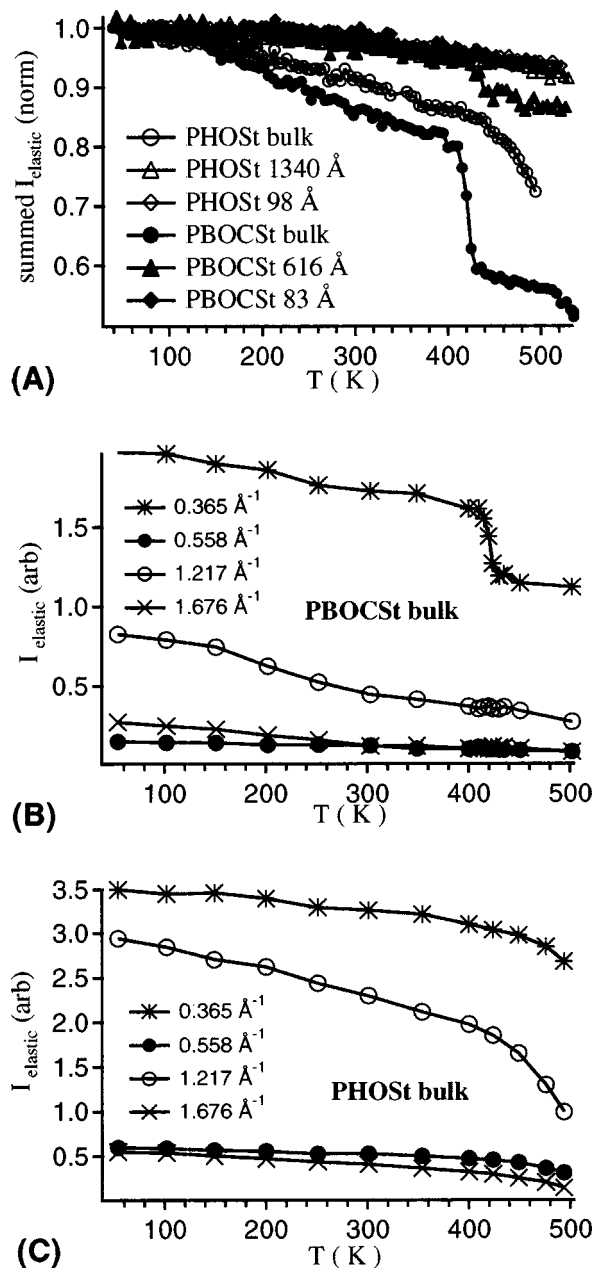


FIG. 2. (a) Changes in total incoherent elastic neutron scattering, normalized to 1 at 50 K, as a function of the temperature for the PBOCSt and PHOSt bulk and thin film samples. Thermal motions lead to decrease in intensity as the temperature increases, and this effect generally diminishes as the film thickness is reduced. (b) and (c) Comparison of the Q dependence of elastic scattering (in arbitrary units) in bulk PBOCSt and PHOSt, respectively, that demonstrates that the marked reduction in scattering near 410 K, coinciding with thermal deprotection of PBOCSt, is limited to low Q detectors. The standard uncertainty in the data is comparable to the size of the data markers.

of the polymer and mass loss is not an issue. Curiously then, the suppression of the discontinuous change upon deprotection with decreasing PBOCSt film thickness suggests that the static structure of the polymer changes as a function of the film thickness. This is a possibility that is currently being explored in greater detail in our laboratory.

From the Q^2 dependence of the elastic intensities we can estimate $\langle u^2 \rangle$ using Eq. (1), as shown in Fig. 3 for the 1340 Å PHOSt films. Despite the limited thin film scattering, there

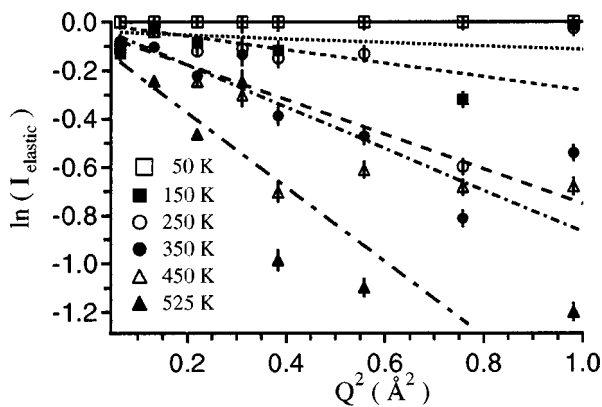


FIG. 3. Natural logarithm of elastic scattering intensity, normalized by the 50 K value, as a function of the square of scattering vector Q^2 for the 1340 Å PHOSt film. Error bars denote the standard uncertainty. Lines indicate the linear fits of the data used to calculate $\langle u^2 \rangle$ according to Eq. (1).

is a noticeable increase in the slope of the linear fits as the temperature increases. This increase in slope corresponds to an increase of $\langle u^2 \rangle$. In these experiments the fitting was limited to the regime where $0.25 \text{ \AA}^{-2} < Q^2 < 1.0 \text{ \AA}^{-2}$. (In separate publications^{10,12} we discuss how the choice of this low Q fitting affects the magnitude of $\langle u^2 \rangle$.) Without repeating those discussions, it is sufficient to realize that fitting the low Q data emphasize the longer-range atomic motions. The Debye–Waller approximation is predicted on harmonic atomic vibrations within a well-defined potential energy well. As we will demonstrate, the longer-range *segmental* motions of the hydrogen containing moieties, such as methyl rotations and/or librations, dominate $\langle u^2 \rangle$ in comparison with the thermal vibrations that are in the spirit of the Debye–Waller approximation. Given these effects, we primarily emphasize the *trends* in $\langle u^2 \rangle$ rather than the absolute magnitude.

Figure 4 demonstrates the $\langle u^2 \rangle$ variations with the temperature and film thickness for both the PHOSt and PBOCSt films. By normalizing the elastic scattering intensities to one at their lowest temperature, $\langle u^2 \rangle$ is defined to be zero at this point for all of the samples. However, significant differences

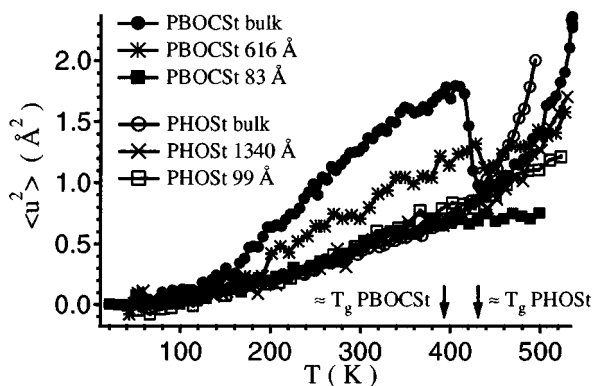


FIG. 4. $\langle u^2 \rangle$ values as a function of the film thickness for PBOCSt and PHOSt, with the vertical arrows indicating the bulk calorimetric T_g of the two materials. Both above and below the T_g bulk there is a strong reduction of $\langle u^2 \rangle$ with the film thickness in PBOCSt, while in PHOSt thin film suppression is only encountered above T_g . The precipitous drop in bulk PBOCSt at 410 K is due to thermal deprotection. The standard uncertainties are less than the size of the data markers.

emerge between the PHOSt and PBOCSt films at elevated temperature. Below the calorimetric glass transition temperature T_g of the bulk materials, the $\langle u^2 \rangle$ values in PBOCSt are much greater than those in PHOSt. Interestingly, the large $\langle u^2 \rangle$ values in the glassy PBOCSt are strongly suppressed as the film thickness decreases. This is not observed in PHOSt in which the relatively small $\langle u^2 \rangle$ values below T_g do not show an appreciable thickness dependence. However, above the bulk T_g strong suppression of $\langle u^2 \rangle$ with decreasing film thickness becomes evident even in this case. With the PBOCSt it is difficult to comment on this region near and above T_g because of complications of thermal deprotection. The thermal deprotection near 410 K results in a sudden decrease in $\langle u^2 \rangle$ for the bulk PBOCSt. This jump in $\langle u^2 \rangle$ becomes less pronounced in the 616 Å films, and absent in the 83 Å films. The implications of these findings will be discussed in greater detail below.

IV. DISCUSSION

A striking feature in Fig. 4 is the large difference of $\langle u^2 \rangle$ in PBOCSt and PHOSt. Immediately *before* thermal deprotection, $\langle u^2 \rangle = 1.8 \text{ \AA}^2$ in the bulk PBOCSt in contrast to 0.7 \AA^2 in bulk PHOSt at the same temperature. With regard to confinement, only in those instances where the motional amplitudes are large, i.e., in PBOCSt, do we see suppression of $\langle u^2 \rangle$ with a decrease in film thickness. Below T_g the $\langle u^2 \rangle$ curves for the bulk, 1340 Å, and the 99 Å PHOSt films are comparable; confinement effects are only observed above the calorimetric T_g when bulk PHOSt displays significantly larger amplitude motions. Unlike PHOSt, PBOCSt displays large amplitude motions below the calorimetric T_g and correspondingly a strong suppression of $\langle u^2 \rangle$ in the glass. This implies that the long-range motions in the polymer film are more susceptible to confinement. Although the data are not presented here, an identical conclusion is obtained when comparing the $\langle u^2 \rangle$ variations in polycarbonate (PC) and polyvinylchloride (PVC) films.^{10,12} PC is analogous to PBOCSt, with large $\langle u^2 \rangle$ values in the glass that show a strong reduction with a decrease in film thickness. In contrast, PVC mimics PHOSt, with small $\langle u^2 \rangle$ values below T_g and no sign of thin film suppression until the bulk T_g is exceeded. In the following, we establish a molecular interpretation for the differences between PBOCSt and PHOSt.

The other prominent feature in Fig. 4 is the large reduction of $\langle u^2 \rangle$ coinciding with the thermally induced deprotection reaction. Volatilization of the protecting group leads to a rapid decrease in the motion amplitude of the PBOCSt. Of course, this is expected from the comparison between the PBOCSt and PHOSt; even below the thermal decomposition temperature there is less “mobility” (small $\langle u^2 \rangle$) in PHOSt. While Fig. 4 looks as if the $\langle u^2 \rangle$ of PBOCSt turns into PHOSt upon deprotection, we stress that this interpretation is not entirely correct. With respect to Fig. 2 we have discussed the volatilization of the protecting group and the accompanying structural changes. In the low Q region this leads to a sudden decrease in the scattering intensity I_{elastic} , and from Eq. (1) where $\langle u^2 \rangle \sim \ln(I_{\text{inc}})/Q^2$, a commensurate decrease in $\langle u^2 \rangle$. To properly account for these changes upon deprotec-

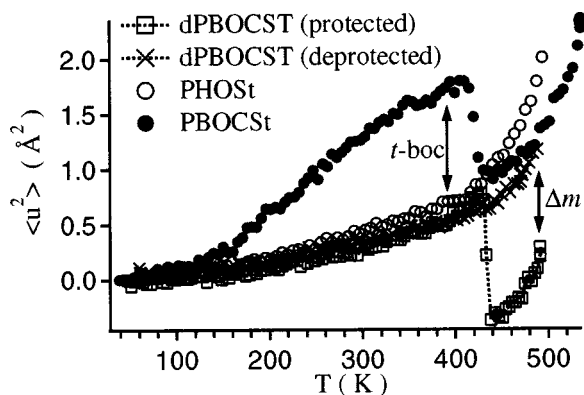


FIG. 5. Comparison of $\langle u^2 \rangle$ in bulk PBOCSt, dPBOCSt (deuterated), and PHOSt. Masking the hydrogen of dPBOCSt that are not present in PHOSt with deuterium (squares) reveals that the large $\langle u^2 \rangle$ in the protected PBOCSt (open circles) originates with the protecting side group that volatilizes upon deprotection ($\langle u^2 \rangle$ in the protected dPBOCSt and PHOSt is similar before deprotection). After deprotection, the mass loss and reduced scattering in dPBOCSt leads to an apparent reduction of $\langle u^2 \rangle$ (squares), which can be corrected for by properly normalizing by the new scattering intensity at 50 K (the \times is once again comparable to PHOSt). The standard uncertainties are less than the size of the data markers.

tion, the data should be *renormalized* by the new scattering intensity at 50 K of the deprotected polymer. Unfortunately, these data were not collected for the samples in Fig. 4. In this respect the fact that $\langle u^2 \rangle$ in bulk PBOCSt drops to a level that appears to be comparable to that of bulk PHOSt upon thermal deprotection is fortuitous. This point will be addressed in greater detail below.

To better understand the dynamical ramifications of the protecting group, it is instructive to compare the $\langle u^2 \rangle$ data for the bulk PHOSt, PBOCSt, and dPBOCSt. In dPBOCSt the phenol ring and the main chain hydrogen, which to first approximation, are structurally equivalent with the PHOSt, dominate the incoherent neutron scattering; the deuterium substitution masks the contribution from the *t*-butyl protecting group. A comparison of these three compounds is presented in Fig. 5. The open and closed circles are the same as the bulk PHOSt and PBOCSt curves shown in Fig. 4 while the squares and \times 's denote the bulk dPBOCSt data. Upon heating from low temperatures, the dPBOCSt is initially protected (squares) and one immediately notices that $\langle u^2 \rangle$ is nearly identical to PHOSt. This directly indicates that the large $\langle u^2 \rangle$ values in PBOCSt are rooted in motions of the *t*-butyl protection group, most probably methyl librations and/or rotations. This also implies that the motions within the protecting group are localized and not cooperative with the rest of the polymer. If there were a high degree of dynamical collectivity, one would expect that the mobility in the side group would impart mobility to the main chain. For example, in poly(methyl methacrylate) it is understood that the side group rotations induce a "wiggle" to the main chain.^{18,19} Likewise, the segmental dynamics of PC below its glass transition temperature are highly collective, and extend across several monomers.^{20,21} If the mobile *t*-butyls were coupled to the dynamics in the main chain and/or the phenyl rings, one would anticipate that $\langle u^2 \rangle$ in dPBOCSt would be greater than in PHOSt. This is clearly not the case, indicating

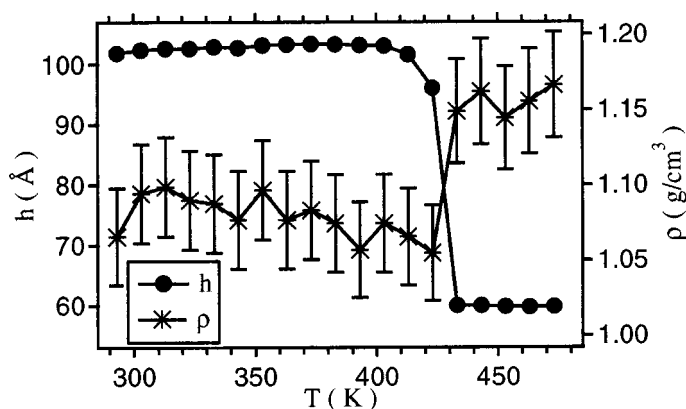


FIG. 6. Decrease in thickness (h) and increase in density (ρ) upon thermal deprotection in an 83 \AA film. The error bars indicating standard uncertainties, if not visible, are less than the size of the data markers.

that the dynamics (faster than 200 MHz) of the protecting group are highly localized. So the distance between the PBOSt and the dPBOCSt curves in Fig. 5, demonstrated by the vertical *t*-boc arrow, gives an estimate of the dynamical contributions by the protection group.

Figure 5 also helps to clarify the role of mass loss and structural changes that occur during thermal deprotection. Just like in bulk PBOCSt, there is a precipitous decrease of $\langle u^2 \rangle$ near 410 K upon initial heating of the dPBOCSt. However, here we see that $\langle u^2 \rangle$ attains unphysical negative values. We can account for this by cooling the deprotected dPBOCSt (\times) back to 50 K, and renormalizing the scattering intensities with the new low temperature values (proper Q dependence). After proper renormalization, the $\langle u^2 \rangle$ values of the deprotected (cooling) dPBOCSt are comparable to those of pure PHOSt. Unlike the hydrogenous PBOCSt, the dPBOCSt sample cell vents directly to vacuum so that, upon deprotection, the gaseous by-products are rapidly removed. This means that the drop in intensity is due to both structure and mass changes (unlike for PBOCSt where the cell was sealed and the gas retained). In the analog in Fig. 2(b) for the dPBOCSt (not shown here), discontinuous changes are observed in all (not just the low Q) the detectors. An indication of how mass loss affects $\langle u^2 \rangle$ can be obtained from the vertical distance, indicated by the Δm arrow, between the protected (squares) and properly normalized deprotected (\times) dPBOCSt curves just beyond thermal decomposition.

The fact that a sudden decrease of $\langle u^2 \rangle$ is not observed in the 83 \AA film PBOCSt film does not imply that the thermal deprotection reaction is suppressed in thin films. This is explicitly demonstrated in Fig. 6 where specular x-ray reflectivity is used to track the thickness as a function of the temperature in a 102 \AA (approximately 83 \AA) film. The 40% decrease in film thickness at elevated temperatures, illustrated elsewhere,²² marks the thermal deprotection reaction. So despite the fact that there is not a sudden drop in $\langle u^2 \rangle$ near 400 K, the reaction is still active in a sub-100 \AA film. More specifically, the suppression of $\langle u^2 \rangle$ in the 83 \AA film reflects suppression of *t*-butyl methyl motion. Also shown in Fig. 6 is the change in film density derived from the critical wave vector Q_c^2 for total reflection of the x rays. The fact that

the density increases as the PBOCSt turns into PHOSt seems qualitatively consistent with the smaller $\langle u^2 \rangle$ values in PHOSt; denser materials would seemingly possess reduced mobility.

Deuterium labeling studies demonstrate that the large $\langle u^2 \rangle$ in PBOCSt reflects motions that are localized to *t*-butyl methyls. However, the ensuing suppression of $\langle u^2 \rangle$ with a decrease in PBOCSt film thickness does not necessarily imply complete immobilization of the methyl groups. A reduction of $\langle u^2 \rangle$ would be observed if the characteristic frequency of the motions were to drop below the 200 MHz instrumental resolution. This scenario is plausible in light of recent methyl group tunneling studies of methyl iodide confined to a controlled-pore glass (pore diameters ranging from 25 to 200 Å).²³ Near absolute zero the quantum mechanical tunneling energies are very sensitive to the potential energy barriers that oppose classical librations and rotations at higher temperatures. These studies demonstrate that confinement induces structural disorder that broadens the distribution of barrier heights and *shifts* the average barrier toward *lower energies*. Lower energy barriers in turn lead to larger amplitude, but lower frequency motions. If the frequency of motions falls below 200 MHz, a decrease in $\langle u^2 \rangle$ (increased elastic scattering) would be observed, irrespective of the larger amplitude displacements.

We previously mentioned that at 410 K (just before the point of thermal decomposition), $\langle u^2 \rangle = 1.8 \text{ \AA}^2$ in bulk PBOCSt. By comparison, $\langle u^2 \rangle$ in the 83 Å PBOCSt film is on the order of 0.7 \AA^2 at the same temperature. One would have to cool the bulk PBOCSt sample to approximately 210 K to find a comparable $\langle u^2 \rangle = 0.7 \text{ \AA}^2$. It is tempting to argue that the thin film dynamics have been shifted by a thermal energy equivalent to 200 K in contrast to that of the bulk. With respect to the fact that the methyl groups are responsible for this large $\langle u^2 \rangle$ in bulk PBOCSt, this concept of a shift is not entirely unreasonable since 200 K is comparable to a 17 meV shift. The energy barrier for methyl rotation of the *t*-butyl group in liquid ethyl tertiary butyl ether [(CH₃)₃COCH₂CH₃] is approximately 128 meV.²⁴ For an order of magnitude approximation, we can assume that *glassy* PBOCSt and *liquid* ethyl tertiary butyl ether have similar energy barriers for rotation. Then the thin film confinement would have appeared to shift the activation energy by a factor of $17/128 = 0.13$. Interestingly, this is comparable to the shift in the methyl iodide rotational barrier from 42 meV in the bulk to 37.3 meV when confined in 50 Å pores,²³ i.e., a factor of 0.11. While this elementary discussion is based on the notion of simple methyl rotation, bear in mind that we have not precisely identified what type of motion in the *t*-butyl group is responsible for the large $\langle u^2 \rangle$. It is highly likely that it is a very complicated combination of methyl rotations, librations, wagging, etc.

Of course, the comparison between methyl iodide and our polymer is exceedingly crude. For methyl iodide in a 50 Å pore, it is easy to envision confinement frustrating the packing the thereby diminishing the intermolecular potentials opposing methyl group rotation. However, in a polymer, where connectivity is an issue, the effect of confinement is not intuitive. On one hand, the reduced dimensionality of a

thin film decreases the degrees of freedom available to a chain, thereby frustrating packing. This is analogous to the small molecules confined to a pore and consistent with reduced potential energy barriers. However, the linear connectivity may also lead to locally parallel chain segments interacting strongly with the substrate in the thin films. It is also possible that the enhanced or forced interactions with the substrate and/or neighboring chains increases the potential energy barriers for methyl group mobility. This scenario would also lead a reduction of $\langle u^2 \rangle$ with a decrease in film thickness. Larger energy barriers lead to higher frequency, but small amplitude motions. Unfortunately, we cannot distinguish between these two very different explanations. This is similar to the earlier discussion of how both structural and dynamic changes may occur as the film thickness is diminished, and on some levels, the two cannot be separated (structure breeds dynamics). Nevertheless, we shall proceed and develop a phenomenological correlation between the reduction of $\langle u^2 \rangle$ and decreased kinetics in these thin lithographic films.

Debye–Waller mean-square displacement reflects the “openness” of a material or the spatial scale over which high frequency motions can occur. For example, $\langle u^2 \rangle$ in a dense crystalline solid, in which very little atomic motion exists, is relatively small in comparison to in the glassy state in which lower density packing heterogeneities are prevalent and local mobility is possible. There have been strong correlations between $\langle u^2 \rangle$ and the electron density heterogeneities, or nanovoids, measured by positron annihilation life spectroscopy.^{25–28} However, the precise relation between $\langle u^2 \rangle$ and the average unoccupied or cavity volume as seen by positron annihilation, sometimes loosely (and often incorrectly) referred to as “free volume,” has not been established. Classical models of mobility suggest that the dynamic properties of a glassy strongly decrease as the free volume V_f approaches a limiting low temperature value, $V_f(T \rightarrow 0) = V_{f,0}$. Specifically, Doolittle²⁹ suggested that the viscosity η varies as $\eta = \eta_0 \exp[-\gamma V_{f,0}/(V_f - V_{f,0})]$ (γ is an adjustable parameter), with a similar form rationalized theoretically by Cohen and Turnbull.³⁰ While in the Doolittle arguments V_f is related directly to the specific volume, it is not unreasonable to anticipate correlations with the microscopic unoccupied volume reflected in $\langle u^2 \rangle$ ($\langle u^2 \rangle^{3/2}$ is comparable to a microscopic volume). In terms of H⁺ or acid mobility, it seems reasonable to anticipate that larger $\langle u^2 \rangle^{3/2}$ volumes would lead to enhanced diffusion.

Recent Lennard-Jones bead-spring simulations of polymer fluids by Starr and co-workers³¹ showed a relation between $\langle u^2 \rangle^{3/2}$ and a well-defined type of free volume. In this interpretation $\langle u^2 \rangle^{3/2}$ corresponds to the mean volume that the center of an atom (bead) can “rattle” within when the surrounding particles are fixed, and this definition further has a rigorous relation to the equation of state for hard sphere fluid.^{32–34} Previous measurements and models support a scaling relation between the viscosity and this well-defined and experimentally measurable type of free volume. For example, Buchenau and Zorn³⁵ empirically showed that the viscosity of liquid and glassy Se exponentially scales with $\langle u^2 \rangle$ through the relationship

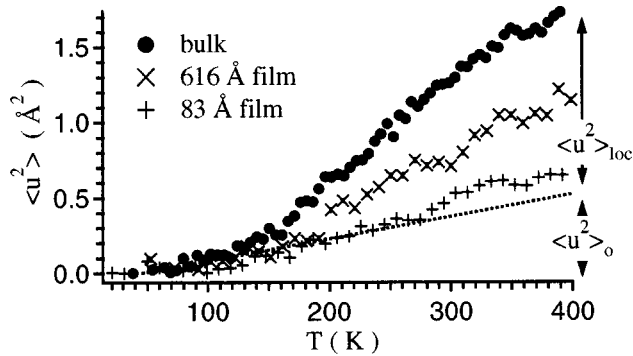


FIG. 7. Thermal evolution of $\langle u^2 \rangle$ in PBCOSt as a function of the film thickness below the thermal decomposition temperature. A linear fit of the bulk data between 40 and 80 K is used to extrapolate an approximation for the harmonic-like vibrational contributions $\langle u^2 \rangle_o$ at elevated temperature. The difference between $\langle u^2 \rangle$ and $\langle u^2 \rangle_o$ is defined as $\langle u^2 \rangle_{\text{loc}}$ (following Refs. 27 and 35). The error bars indicate the standard uncertainty in $\langle u^2 \rangle$.

$$\eta = \eta_o \exp\left(\frac{\langle u^2 \rangle_o}{\langle u^2 \rangle_{\text{loc}}}\right), \quad (2)$$

where $\langle u^2 \rangle_{\text{loc}}$ is defined as the difference in $\langle u^2 \rangle$ between the crystalline and the liquid/glassy states. Likewise, Kanaya and co-workers have recently demonstrated the utility of Eq. (2) in describing the viscosity of liquid and glassy polybutadiene.²⁷ To support these two experimental examples, relations, comparable to those of Eq. (2) have been predicted theoretically by a number of authors,^{36–38} and at some level a large $\langle u^2 \rangle$ should lead to enhanced transport.

If one assumes that $\langle u^2 \rangle$ influences the mobility of H^+ in a PBCOSt film, then Eq. (2) suggests that the decrease of $\langle u^2 \rangle$ with film thickness corresponds to a decrease in the H^+ diffusion coefficient, assuming an Einstein-like dependence of $\eta \sim kT/aD$. This leads to estimates of the relative change of η and D due to confinement:

$$\frac{\eta_{\text{film}}}{\eta_{\text{bulk}}} = \frac{D_{\text{bulk}}}{D_{\text{film}}} = \exp\left(\frac{\langle u^2 \rangle_o}{\langle u^2 \rangle_{\text{loc, film}}} - \frac{\langle u^2 \rangle_o}{\langle u^2 \rangle_{\text{loc, bulk}}}\right), \quad (3)$$

assuming that $\langle u^2 \rangle_o$ is unchanged by confinement. Unfortunately, PBCOSt is not like Se in that it can be easily crystallized, so $\langle u^2 \rangle_{\text{loc}}$ cannot be directly measured. However it is reasonable to estimate the level of harmonic contributions at elevated temperature by fitting the bulk $\langle u^2 \rangle$ data between 40 and 80 K to a linear function and extrapolating to high temperature. In this low temperature region, the atomic motions are nearly harmonic, like a crystal, so that $\langle u^2 \rangle_{\text{loc}}$ can be approximated as the difference between $\langle u^2 \rangle$ at any temperature and linearly extrapolated from the low temperature behavior. Figure 7 demonstrates how this approximation is made for the PBCOSt films. As implied by Eq. (2) there is also a critical displacement $\langle u^2 \rangle_o$ at which the viscosity in the film becomes exceedingly large. With regard to the acid transport problem, we define $\langle u^2 \rangle_o$ to be this high temperature extrapolation of harmonic behavior. The implication of this definition is that the magnitude of $\langle u^2 \rangle$ facilitates transport of the H^+ ; i.e., there would be no H^+ transport if PBCOSt could be made into a harmonic, crystalline-like solid.

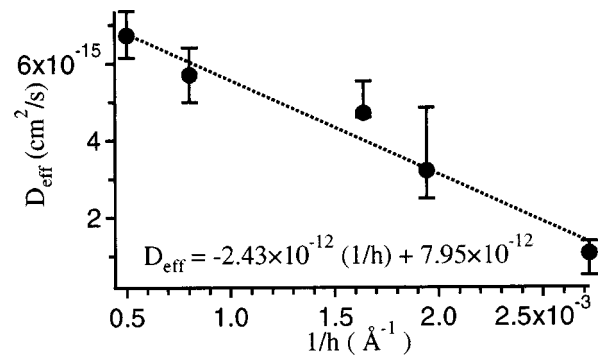


FIG. 8. Effective reaction front diffusion coefficient (and standard uncertainties) reported elsewhere (Ref. 39), as a function of the inverse film thickness. The linear function indicated by the dotted line is used to estimate D_{eff} in the limit of infinite thickness (i.e., a bulk sample).

From the estimates of $\langle u^2 \rangle_o$ and $\langle u^2 \rangle_{\text{loc}}$, Eq. (3) can be used to predict the corresponding decrease in the effective H^+ diffusion coefficient of the thin films. The $D_{\text{bulk}}/D_{\text{film}}$ comparisons are made at 383 K based on previous estimates for the velocity of the deprotection reaction front in model PBOCSt/PHOSt bilayers.³⁹ Without going into details of these experiments, a thick film of PHOSt containing the photoacid generating molecules is spun cast over the top of a thin PBOCSt layer. The entire bilayer is exposed to UV radiation to generate photoacids in the top layer, and then baked to facilitate acid diffusion into and deprotection of the PBOCSt underlayer. By measuring how far the reaction front propagates into the PBOCSt underlayer as a function of the bake time, it is possible to extract an effective reaction front diffusion coefficient D_{eff} . Figure 8 summarizes the D_{eff} deviation as the thickness of the PBOCSt underlayer diminishes. Qualitatively, the results are in agreement with the $\langle u^2 \rangle$ predictions; transport of H^+ diminishes as the PBOCSt film thickness decreases.

The comparison between the D_{eff} and the $\langle u^2 \rangle$ predictions can be made more quantitative by extracting a bulk D_{eff} from Fig. 8. It appears that, as the film thickness increases, D_{eff} approaches a limiting value for the bulk. We extract this limiting value by inverting the ordinate and plotting D_{eff} as a function of $1/h$. In this representation the data can be fit with a straight line and from the intercept at $1/h=0$, one obtains a bulk D_{eff} of $7.95 \times 10^{-12} \text{ cm}^2/\text{s}$. Using this fitted value for bulk normalization, the $D_{\text{bulk}}/D_{\text{film}}$ values are plotted as a function of h in Fig. 9. The closed circles indicate D_{eff} values reported elsewhere³⁹ while \times denotes predictions from the $\langle u^2 \rangle$ measurements. Clearly, there is reasonable agreement between the two data sets, suggesting that the reduction of $\langle u^2 \rangle$ in the thin film is linked to suppression of the reaction front propagation kinetics. We note that there are only two data points for the $\langle u^2 \rangle$ predictions, and that one of these films is significantly thinner than any of the measured D_{eff} samples. Nonetheless, the qualitative trends in the limited data are similar.

Based on a previous set of $\langle u^2 \rangle$ measurements in thin polycarbonate films, it is reasonable to expect that $\langle u^2 \rangle$ increases exponentially with the inverse of film thickness.¹⁰ While we only have three points by which to establish this

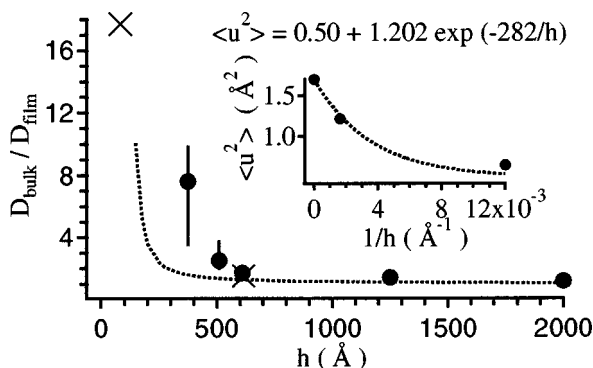


FIG. 9. Ratio of the bulk to thin film diffusion coefficient plotted as a function of the film thickness. Circles represent the data presented in Fig. 7 while \times denotes values predicted from the $\langle u^2 \rangle$ data using Eq. (3). The inset displays the $\langle u^2 \rangle$ data as a function of the inverse film thickness, fit to a function form of $\langle u^2 \rangle = A \exp(B/h)$. The dotted line in the main portion indicates the predicted ratio using the fitting results and Eq. (3). The error bars indicate the standard uncertainty in the experimental data.

relation, we attempt to fit our $\langle u^2 \rangle$ data at 383 K to the form of $\langle u^2 \rangle = A \exp(B/h)$. In this case we chose prefactors A and B so that two boundary conditions are met: $\langle u^2 \rangle = 1.702$ at $1/h = 0$ and $\langle u^2 \rangle = 0.50 = \langle u^2 \rangle_0$ at $1/h = \infty$. This ensures that the fit reaches the proper bulk value in an infinitely thick film, and that it does not drop below what we estimated to be the lower harmonic limit if the PBOCSt were to exist as a crystal-like state. This is reasonable given that molecules near a surface tend to layer, with crystalline-like radial distribution functions.⁴⁰ The inset in Fig. 9 displays the results of this fit, and indicates reasonable agreement with the experimental data. Although more data are required to increase the reliability of the fit, we can use the fitted values of $\langle u^2 \rangle$ to predict the $D_{\text{bulk}}/D_{\text{film}}$ ratio, indicated by the dotted line in Fig. 9. While the deviations from bulk-like behavior appear to be shifted toward slightly thinner films in the $\langle u^2 \rangle$ predictions, the general shape of the curve is similar to the measured data. This suggests that our simplistic model may be pointing to the correct underlying physics for retardation of the reaction front in exceedingly thin films.

To summarize, we have used elastic incoherent neutron scattering to parameterize changes in the atomic/molecular mobility in PBOCSt and PHOST films as a function of the thickness. Changes in the 200 MHz and faster dynamics are estimated in terms of a harmonic oscillator and the Debye–Waller factor mean-square atomic displacement $\langle u^2 \rangle$. The large $\langle u^2 \rangle$ values in PBOCSt appear to be localized to methyls of the *t*-butyl protecting group. In comparison, the amplitude of the dynamics of the deprotected analog polymer, PHOST, is notably reduced with much smaller $\langle u^2 \rangle$ values in the glassy state. When confined to thin films, the large $\langle u^2 \rangle$ in the PBOCSt is strongly suppressed as the film thickness diminishes, especially in the glassy state. This is in stark contrast to PHOST in which there is no suppression of $\langle u^2 \rangle$ in the glassy state as a function of the film thickness. In bulk glass forming fluids, reductions of $\langle u^2 \rangle$ have been used to describe increases in the viscosity. Likewise, we have used the thin film reduction of $\langle u^2 \rangle$ to predict an exponential reduction of H^+ mobility in the thin PBOCSt films. Independ-

ent measurements support these proposed relations, however, additional measurements and theoretical interpretation are required to generalize these very promising initial results.

ACKNOWLEDGMENTS

Funding for this work came from the DARPA Advanced Lithography Program, Grant No. N66001-00-C-8803. The neutron scattering activities were made possible in part by the National Science Foundation, under Agreement No. DMR-0086210. Brain Trinqué, Sean Burns, and C. Grant Willson synthesized the deuterium PBOCSt reported in Ref. 15. The authors also thank Dave Vanderhart, Rob Dimeo, and Dan Neumann for their valuable discussions and critical review of the manuscript.

- ¹J. Crank and G. S. Park, *Diffusion in Polymers* (Academic, London, 1968).
- ²P. Neogi, *Diffusion in Polymers* (Dekker, New York, 1996).
- ³L. G. F. Stuk, *J. Polym. Sci., Part B: Polym. Phys.* **28**, 127 (1990).
- ⁴M.-B. Haag, W. J. Koros, and J. C. Schimidhauser, *J. Polym. Sci., Part B: Polym. Phys.* **32**, 1625 (1994).
- ⁵M. Ponitsch, P. Gotthardt, A. Gruger, H. G. Brion, and R. Kirchheim, *J. Polym. Sci., Part B: Polym. Phys.* **35**, 2397 (1997).
- ⁶C. L. Soles and A. F. Yee, *J. Polym. Sci., Part B: Polym. Phys.* **38**, 792 (2000).
- ⁷R. A. L. Jones and R. W. Richards, *Polymers at Surfaces and Interfaces* (Cambridge University Press, Cambridge, UK, 1999).
- ⁸A. Karim and S. Kumar, *Polymer Surfaces, Interfaces, and Thin Films* (World Scientific, Singapore, 1999).
- ⁹R. A. Jones, *Curr. Opin. Colloid Interface Sci.* **4**, 153 (1999).
- ¹⁰C. L. Soles, J. F. Douglas, W.-I. Wu, and R. M. Dimeo, *Phys. Rev. Lett.* **88**, 037401 (2002).
- ¹¹C. L. Soles, E. K. Lin, J. L. Lenhart, R. L. Jones, W.-I. Wu, D. L. Goldfarb, and M. Angelopoulos, *J. Vac. Sci. Technol. B* **19**, 2690 (2001).
- ¹²C. L. Soles, J. F. Douglas, W.-I. Wu, and R. M. Dimeo (unpublished).
- ¹³Certain commercial equipment and materials are identified in this paper in order to specify adequately the experimental procedure. In no case does such identification imply recommendation by the National Institute of Standards and Technology nor does it imply that the material or equipment identified is necessarily the best available for this purpose.
- ¹⁴J. M. Frechet, E. Eichler, H. Ito, and C. G. Willson, *Polymer* **24**, 995 (1983).
- ¹⁵E. K. Lin *et al.*, *Science* **297**, 372 (2002).
- ¹⁶P. M. Gehring and D. A. Neumann, *Physica B* **241–243**, 64 (1998).
- ¹⁷G. Floudas and P. Stepanek, *Macromolecules* **31**, 6951 (1998).
- ¹⁸A. F. Yee and M. T. Takemori, *J. Polym. Sci., Polym. Phys. Ed.* **20**, 205 (1982).
- ¹⁹K. Schmidt-Rohr, A. S. Kulik, H. W. Beckham, A. Ohlemacher, U. Pawelzik, C. Boeffel, and H. W. Spiess, *Macromolecules* **27**, 4733 (1994).
- ²⁰J. Y. Jho and A. F. Yee, *Macromolecules* **30**, 6302 (1997); P. L. Lee, T. Kowalewski, M. D. Poliks, and J. Schaefer, *ibid.* **28**, 2476 (1995); J. M. Goetz, J. Wu, A. F. Yee, and J. Schaefer, *ibid.* **31**, 3016 (1998).
- ²¹F. J. Horth, K. J. Kuhn, J. Mertes, and G. P. Hellmann, *Polymer* **33**, 1223 (1992).
- ²²J. L. Lenhart, R. L. Jones, E. K. Lin, C. L. Soles, W.-I. Wu, D. L. Goldfarb, and M. Angelopoulos, *J. Vac. Sci. Technol. B* **20**, 704 (2002).
- ²³R. M. Dimeo and D. A. Neumann, *Phys. Rev. B* **63**, 014301 (2001); R. M. Dimeo, D. A. Neumann, Y. Glanville, D. B. Minor, *ibid.* (in press).
- ²⁴R. D. Sueram, F. J. Lovas, W. Pereyra, G. T. Fraser, and A. R. Hight Walker, *J. Mol. Spectrosc.* **181**, 67 (1997).
- ²⁵V. N. Novikov, A. P. Sokolov, B. Strube, N. V. Surovstev, E. Duval, and A. Mermert, *J. Chem. Phys.* **107**, 1057 (1997).
- ²⁶J. Bartos, P. Bandzuch, O. Sausa, K. Kristiakova, J. Kristiak, T. Kanaya, and W. Jenninger, *Macromolecules* **30**, 6906 (1997).
- ²⁷T. Kanaya, T. Tsukushi, K. Kaji, J. Bartos, and J. Kristiak, *Phys. Rev. E* **60**, 1906 (1999).
- ²⁸K. L. Ngai, L.-R. Bao, A. F. Yee, and C. L. Soles, *Phys. Rev. Lett.* **87**, 215901 (2001).
- ²⁹A. K. Doolittle, *J. Appl. Polym. Sci.* **22**, 1471 (1951).
- ³⁰M. H. Cohen and D. Turnbull, *J. Chem. Phys.* **31**, 1164 (1959).

- ³¹F. W. Starr, S. Sastry, J. F. Douglas, and S. C. Glotzer, Phys. Rev. Lett. (in press).
- ³²W. G. Hoover, W. T. Ashurst, and R. Grover, J. Chem. Phys. **57**, 1259 (1972).
- ³³R. J. Speedy, J. Chem. Soc., Faraday Trans. 2 **73**, 714 (1977); **75**, 1643 (1980); **76**, 693 (1980); **77**, 329 (1981).
- ³⁴H. Reiss and A. Dell Hammerich, J. Phys. Chem. **90**, 6252 (1986); R. J. Speedy and H. Reiss, Mol. Phys. **72**, 999 (1991); **72**, 1015 (1991).
- ³⁵U. Buchenau and R. Zorn, Europhys. Lett. **18**, 523 (1992).
- ³⁶R. W. Hall and P. G. Wolynes, J. Chem. Phys. **86**, 2943 (1987).
- ³⁷J. C. Dyre, N. B. Olsen, and T. Christensen, Phys. Rev. B **53**, 2171 (1996).
- ³⁸U. Zurcher and T. Keyes, Phys. Rev. E **60**, 2065 (1999).
- ³⁹D. L. Goldfarb, M. Angelopoulos, E. K. Lin, R. L. Jones, C. L. Soles, J. L. Lenhart, and W.-I. Wu, J. Vac. Sci. Technol. B **19**, 2699 (2001).
- ⁴⁰J. Israelachvili, *Intermolecular and Surface Forces*, 2nd ed. (Academic, London, 1992).